Experimental Investigations of Active Flow Control Using a Piezo Adaptive Blade in a Compressor Cascade Under Periodic Boundary Conditions with High Strouhal-Number

Tobias Werder[(✉)], Lukas Kletschke, and Robert Liebich

Technische Universität Berlin, Straße des 17. Juni 135, 10623 Berlin, Germany
tobias.werder@tu-berlin.de

Abstract. As a consequence of constant volume combustion in gas turbines, pressure waves are generated that propagate upstream the main flow into the compressor system are generated leading to incidence variations. Numerical and experimental investigations of stator vanes have shown that Active Flow Control by means of adaptive blade geometries is beneficial when such periodic incidence variations occur. A less susceptible to stall and choking for compressors dealing with periodic disturbances can be achieved. Experimental investigations with high Strouhal numbers using such a method have not yet been done in order to demonstrate the effects. Therefore, this work investigates a linear compressor cascade that is equipped with a piezo-adaptive blade structure utilizing macro-fiber-composite actuators. A throttling device is positioned downstream of the trailing edge to emulate an unsteady combustion process. Periodic transient throttling events with Strouhal numbers up to 0.144 were being investigated due to incidence changes. Consequently, pressure fluctuations on the blade's surface occur, having a significant impact on the pressure recovery downstream of the stator cascade. Experimental results of harmonically actuating the piezo-adaptive blade with Strouhal numbers of up to 0.72 show that the impact of disturbances at resonance can be nearly reduced to zero. Therefore, the blade design must be matched to the type of disturbances to achieve further improvements in the technology.

Keywords: Piezo · Blade · Flow control · Active · AFC · CVC · Compressor

1 Introduction

Modern gas turbines are highly efficient and powerful machines, which are used in a variety of applications, e.g. airplane propulsion and power plants to generate electrical energy and heat. Efforts raising the efficiency of gas turbines

for reasons of environmental and economical issues are continuously increasing while nowadays small improvements usually demand substantial investments in component research and development. A major breakthrough for the overall gas turbine efficiency cannot be expected without disruptive technologies.

One of those technologies that aims at a significant increase in efficiency is constant volume combustion (CVC). By applying a pressure gain combustion process, an inherently higher thermodynamic efficiency can achieved. Nevertheless, such improvement comes at the cost of unsteady effects, such as pressure fluctuations originating from the combustor. This leads to implications for compressor and turbine, such as incidence variations with an increased risk of stall or choke. An effective way of dealing with any kind of disturbances in turbomachinery is Active Flow Control (AFC). In the case of a CVC, AFC can reduce the impact of disturbance and ensure robust and stable operation.

The application of AFC may present one means to gain higher efficiency. Many of them use pressurized air to manipulate the passage airflow or conditions on the blade's surface. Staats and Nitsche [1] and Steinberg et al. [2] investigated a compressor cascade with periodic unsteady outflow conditions. Fluidic actuators on the blade's suction side and the adjacent sidewall near the leading edge were used to control static pressure distribution on the blade's surface and the pressure rise as well as the total pressure loss coefficients in the wake. A separation suppression of the flow and less sidewall effects lead to effective disturbance rejection.

Another AFC method comprises an adaptive blade geometry. Hammer et al. [3] showed that adjustable shapes can increase the operating range of a compressor stage and thus enable a more stable operation of the stage. They investigated a mechanically adjustable front part of piezo adaptive blades and showed that this method can enlarge the operating range of a compressor stage. Phan et al. [4] had shown in a numerical study that an oscillating leading edge of a piezo adaptive blade can reduce the negative effects of oscillating incidences, e.g. a suction peak, and thus the associated higher susceptible of stall. Furthermore, they designed and tested a similar adaptive blade design with Macro Fiber Composite Actuators (MFC) for cascade experiments [5]. Krone et al. [6] investigates the benefits of MFC in a linear cascade to extend the workspace as well. An other moving leading edge investigation from Ko et al. [7] is done to control the reverse flow of a blade.

An adaptive blade with oscillating leading edge in an open wind tunnel with throttle-induced pressure fluctuations was already investigates before by [8]. But the case of high STROUHAL-numbers in actuation compared with throttling has not yet been examined experimentally. The present work experimentally demonstrates the benefits of this system under conditions similar to those of CVC-capable gas turbines.

2   Theoretical Considerations

The theoretical background for the idea of harmonically varying the shape of the front part of a compressor vane will be shown in this section. A compressor vane is normally designed for one angle of attack α with minimal angle of incidences

i. Under these normal circumstances, minor losses are to be expected for a little range of incidences. However, for operating a gas turbine with CVC a fluctuation in angle of incidence of up to 3 degrees occurs [1].

This incidence called i_{CVC} leads to much greater losses, which can be compensated by generating a dynamic blade angle $\beta = \omega t + \varphi$, which represents the stationary incidence angle i_{stat}. The ω stands for the angular frequency of excitation ($\omega = 2\pi f_a$), t is time and φ is a phase shift, resulting in an so called blade incidence i_{blade} described in Eq. 1. If a blade with i_{blade} is designed in such a way that i_{res} disappears, a disturbance-free flow around the blade is obtained. For a slowly moving blade in a undisturbed flow, the angle of incidence changes in a more stationary manner as described in Eq. 3, comparable to an airplane wing or moving blades in stationary gas turbines for start-up operations, turbines for ramp-up operations or load changes. If the blade – or in this case the leading edge – moves fast, however, we can not neglect the induced velocity perpendicular to the chord. This velocity leads to an angle of incidence i_{dyn} in addition to the stationary i_{stat}. It will be called dynamic incidence henceforth and is described in Eq. 4. The negative sign in Eq. 1 designates from the definition of the direction of angles. In this equation $A(\omega)$ is the dynamic displacement amplitude of the leading edge at an applied harmonic voltage to a MFC Actuator of $V = \hat{V} sin(\omega t)$ with excitation frequency ω. This amplitude changes like a forced harmonic oscillator. The oscillation is described in Eq. 5 with natural frequency ω_0. The function $f(\hat{V})$ in Units of mm describe a magnification of $A(\omega)$ for different excitation amplitudes $\hat{V}$ in Units of volts. The parameter D stands for structural damping and A_0 is the offset of amplitude considering a different stiffness in up and down movement, if necessary. Measurements of i_{CVC} result for an applied case in a blade design and blade material that gives the parameters for the moving function of the blade $A(\omega)$ and a driving pattern to adjust the phase shift in an closed loop control system. In a best case scenario with perfectly matched parameters i_{res} vanishes at CVC.

$$i_{blade} = i_{stat} - i_{dyn}, \tag{1}$$

$$i_{res} = i_{CVC} - i_{blade}, \tag{2}$$

$$i_{stat} = \arcsin\left(\frac{A(\omega)\sin(\omega t + \varphi) + A_0}{c}\right), \tag{3}$$

$$i_{dyn} = \arctan\left(\frac{A(\omega) \cdot \omega \cdot \cos(\omega t + \varphi)}{v_\infty}\right), \tag{4}$$

$$A(\omega) = \frac{f(\hat{V})}{\sqrt{(1 - \eta^2)^2 + (2D\eta)^2}}, \text{ with } \eta = \frac{\omega}{\omega_0}. \tag{5}$$

Figure 1 shows changes in relative velocity and incidence with their relation to an induced velocity w that occurs because of the moving tip.

Assuming a simple linear oscillator and values given in Table 1 referring to our system described later, the calculated frequency response of the incidence angles and the spectrum of movement of the blade's leading edge are shown in Fig. 2. What can be seen in Fig. 2 is an increasing magnitude at resonance causing the
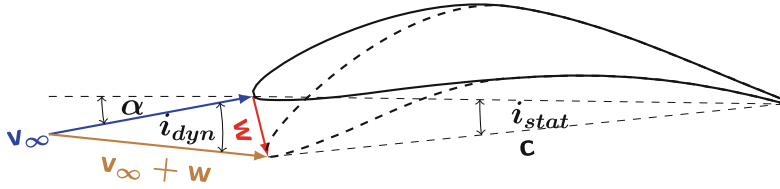
Fig. 1. Schematic velocity triangle of dynamically deformed blade

Table 1. Data of calculation

Parameter	Symbol	Value	Unit
Chord length	c	150	mm
Inflow velocity	v_∞	25	m/s
Angular frequency of blade	ω_0	122π	rad/s
Expected amplitude of excitation driven by MFC	$f(\hat{V})$	0.03	mm
Structural damping ratio of the blade	D	0.015	–

oscillations of the blade. The amplitudes of i_{res} dominate over all frequencies. The reason is the phase shift between i_{stat} and i_{dyn}. For low frequencies the phase angle φ is zero neglecting the influence of the dynamic incidence. At high frequencies the dynamic incidence prevails due to the very low amplitude but high momentum of the blade's leading edge. Looking at the angle of maximum amplitudes given by

$$\frac{\partial i_{res}}{\partial t} = 0, \tag{6}$$

$$\Rightarrow \varphi_{max} = \arctan(\frac{-2v_\infty}{c\omega}). \tag{7}$$

at which these incidences occur, there is a phase shift from $\frac{\pi}{2}$ to π pictured in Fig. 2 below. This is due to the zero phase shift of sinus for low and a phase shift of $\frac{\pi}{2}$ for cosinus at high frequencies. Near resonance, it considering both phase angles is important. This considerations are necessary to understand the fact that a pressure signal from a measurement can be separated into different transfer functions. For an open loop control system the only variables here are the voltage and frequency of the excitation. Figure 3 shows the signal path of the measurement system in a block diagram. The figure shows a schematic of signal processing by using transfer functions. All of these subsystems have to be identified to obtain the actual behavior of the blade and the correct interpretation of the measured signals. The four subsystems are represented as

- $\mathbf{G}_b$ as the transfer function for blade motion,
- $\mathbf{G}_i$ as the transfer function for the angles of incidence,
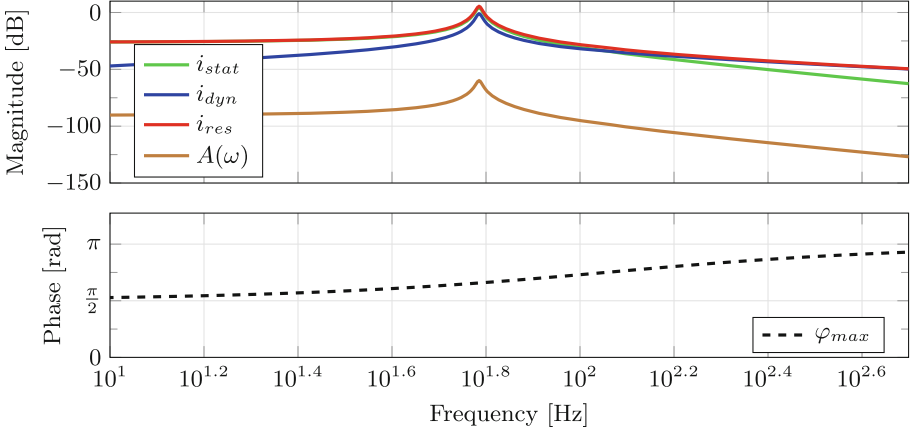
Fig. 2. Frequency response of the different incidence angles and phase shift of i_{res} for an blade design made of aluminum and parameters from Table 1
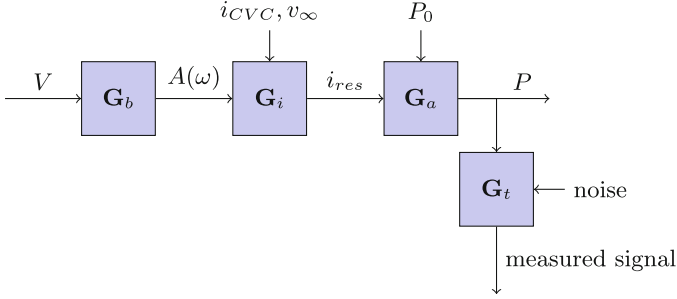

Fig. 3. Signal path in block diagram with different transfer functions of the whole measurement

– $\mathbf{G}_a$ for the ambient air and
– $\mathbf{G}_t$ as the transfer function of a tube from the blade surface to the sensor.

3   Experimental Setup

All experimental results in this paper are based on a similar setup to [8]. They were obtained from a low-speed compressor cascade, which consists of nine linearly arranged compressor stator blades (see Fig. 4a). This design guarantees symmetric conditions at the measurement passage, while minimizing the influence on the top and bottom walls. Measurements and actuation were carried out on blade number 5 and its wake. A boundary layer suction device was installed on the top and the bottom side walls of the cascade and adjusted such that the static inflow pressure is uniform. Static pressure taps at half the chord length c
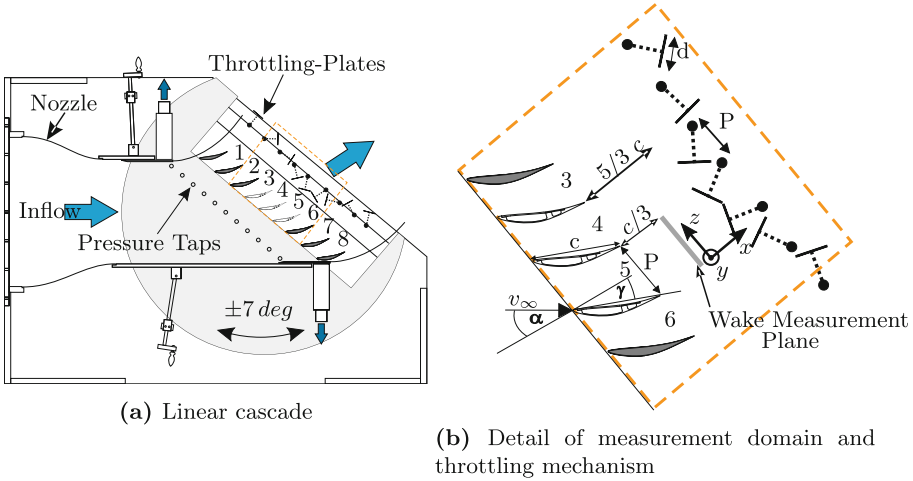
(a) Linear cascade

(b) Detail of measurement domain and throttling mechanism

Fig. 4. Experimental setup

upstream of the blade's leading edge measured the pressure distributed over the entire passage width. For preliminary experiments with this blade, the inflow angle can be varied up to ±7°. The Controlled Diffusion Airfoil (CDA) has a deflection angle of 26.4°. It is designed as a laminar profile shifting the laminar-to-turbulent boundary layer transition further downstream and thus reducing the amount of secondary flow in the cascade as described in [9]. Three of the nine blades were designed adaptable for nearly symmetrical conditions in passage 4 and 5, but only one is used in this investigation to depict the potential of the design. The drive of all three blades caused a resonance failure and has to be investigated by aeroelastic specialists before an other drive with more than one adaptive blade will be done.

Table 2. Data of cascade

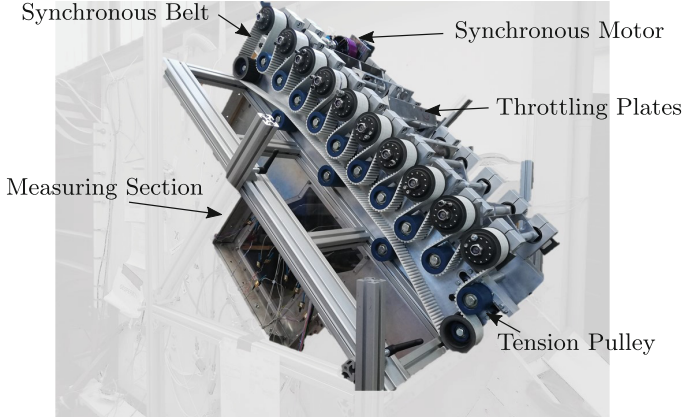| Parameter	Symbol	Value	Unit
Pitch	P	102	mm
Plate depth	d	55	mm
Plate height	L_p	300	mm
Stagger angle	γ	30	deg
Inlet flow angle	α	47	deg
Reynolds number	Re	$2.5 \cdot 10^5$	–
Mach number	Ma	0.07	–
Blade height	L	300	mm

Fig. 5. Throttling device

Figure 4 shows the installed throttling device. It was located at a distance of $5/3\,c$ in the wake of the cascade. The device consists of nine throttling blades eccentrically mounted on nine rotor shafts driven by a synchronous motor. A synchronous belt with tension pulley ensures the exact positioning of the throttling blades and an exact blade-to-blade sequence without collisions, see Fig. 5. The throttling blades block the flow through the passages being arranged in an angle of 45 degrees to each other. The blockage area covers 95% of the passage area. The permanent blockage of the entire device without driving amounts to 25 % of the cascade's wake. All plates rotating in the same direction so the throttling pattern is 1-2-3-4-5-6-7-8-1. Thus it blocks one passage after the other and again from the start. Although the device is designed for frequencies up to $f_c = 100$ Hz, the highest driving frequency here is unfortunately about 25 Hz because of not existing safety system for "plate of" events.

All measurements were taken at a REYNOLDS number of $Re = 2.5 \cdot 10^5$ and an averaged inflow velocity of $v_\infty = 25$ m/s. This can be expressed in the STROUHAL number defined by

$$Sr = \frac{f\,c}{v_\infty} \tag{8}$$

of $Sr = 0.6$ with the throttling frequency being $f = f_c$, the chord length of the blade c and the inflow velocity v_∞. At machine scale this would correspond to throttling frequencies of approx. $f_c = 1575$ Hz at Mach number of $Ma = 0.4$ and a chord of $c = 0.08$ m, which will represent a drive of a Pulse Detonation Combustion (PDC) with a tube length of about 0.5 m. These values represent an industrial high pressure compressor stage [10] and a PDC operation frequency has been shown by Asahare et al. [11]. In the presented work, measurements with STROUHAL numbers from 0.012 to 0.12 for throttling with $f_c = 2...24$ Hz, and $Sr = 0.006...0.72$ for actuation frequencies of $f_a = 1...120$ Hz were performed. These high frequencies could occur at Rotating Detonation Combustion (RDC)

as shown in the work of Anand et al. [12]. All relevant parameters of the passage are summarized in Table 2.

3.1   The Piezo-Adaptive Compressor Stator Vane

An adaptive blade structure with a hollow design utilizing MFC actuators (see Fig. 6 and Table 3) is used to generate leading edge deflections. It is made of aluminum. When actuated harmonically in a sinusoidal form with a supply voltage of up to $V_{max} = \pm 500$ V, the MFCs cause a deformation of the leading edge and thus can react to incidence variation. The actuated front part of the blade changes the blade's designed inflow blade angle by up to 5 deg. The design ensures leading edge pitching like a harmonic oscillator in the region below the second natural frequency. In consequence, the pressure distribution and flow conditions are changed because of incidence variations of values up to 3 deg expected according to Eq. 1. The actuated blade itself consists of three separately manufactured parts: the suction side part including the leading and trailing edge as well as the mounting holes, the pressure side part to generate a structural gap to allow high deflections at the leading edge, and a cover on the pressure side for a supply cable channel. Deformation of the blade's front part is mechanically achieved by stretching and compressing the adhesive-bonded MFCs. This results in a structural bending moment causing a deflection of the leading edge and the whole front part. The structural gap leads to a step on the pressure side and thus in an transition of the flow in it's region an a bit more wide wake depression [5], but the pressure side flow is very stable so that the flow does not detach before the second eigenmode occurs. To measure the angle of incidence caused by the moving tip during wind tunnel measurements we added two strain gauges on the inner side of the suction surface near the mount. These sensors are only measuring strain at the point of application. To obtain the tip deflection, calibration of these sensors is first required. For the calibration, a test rig has been designed to validate the blade's structural properties before using in the cascade. This rig allows clean measurements of the frequency response, structural life time, natural frequencies and shapes without any influence from flow. The rig was mounted on a massive damped base for vibration isolation. The blade was mounted using the holes on the suction side part comparing to the
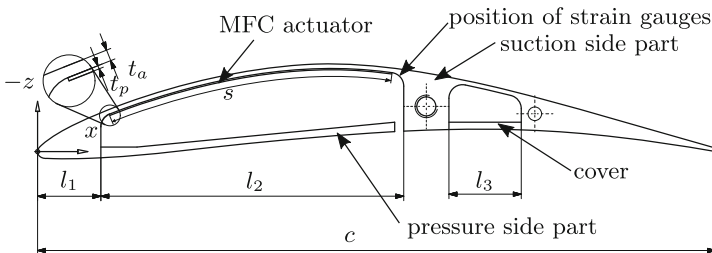

Fig. 6. Design of piezo blade

mounting in the cascade. In addition, the rear part was clamped, so that there is no additional influence of its vibration. The clamping has no effect on the firs natural mode and frequency so it is comparable with the mount in the cascade. This test rig enables oscillation measurements of the blade's front part only. A laser triangulation sensor as well as an eddy current sensor were used for leading edge displacement measurements under MFC actuation to calibrate the strain gauges. The frequency responses at various supply voltages were measured.

Table 3. Data for the Piezo Blade

Parameter	Symbol	Value	Unit
Nose	l_1	14	mm
Hollow part length	l_2	67	mm
Supply cable channel	l_3	16	mm
Patch length	s	67	mm
Patch thickness	t_p	0.3	mm
Blade active part thickness	t_a	1	mm

4   Measurement Methods

The value of interest for a vane is the static pressure distribution on the surface given by the C_P value

$$C_P = \frac{p - p_\infty}{q}. \tag{9}$$

Where p is the local static pressure on the blade's surface, p_∞ the static inflow pressure measured at the wall, and q the dynamic inflow pressure given by

$$q = \frac{\rho}{2} v_\infty^2, \qquad \text{with } \rho = \frac{m\, p_{amb}}{RT}, \tag{10}$$

measured at an undisturbed position at the end of the nozzle outlet of the channel, see Fig. 4a. Here is m the molar mass of air, R is the general gas constant and T is temperature. The value v_∞ is the undisturbed inflow velocity and ρ stands for the density of the medium, which in this case is air. The values for p_{amb} and T were also measured. For an inflow velocity of $v_\infty = 25$ m/s, calculated from Eq. 10, and a density of $\rho = 1.25$ kg/m³, a Mach number of $Ma < 0.3$ applies throughout the range. Figure 7 shows the pressure distribution of measurement data from the adaptive blade and numerical results at Reynolds number of $Re = 2.5 \cdot 10^5$. What can be seen is a good match of the measurement with the numerically calculated ones. A slight deformation of the blade at leading edge occurred by having a look on tap no. 17. No stagnation was not measured, but a negative static pressure. This means that the nose was moving towards the suction side. Also, the separation is shifted downstream, but the pressure

gain is almost the same. Tap No. 15 is marked because all following results are shown as an example for this tap.
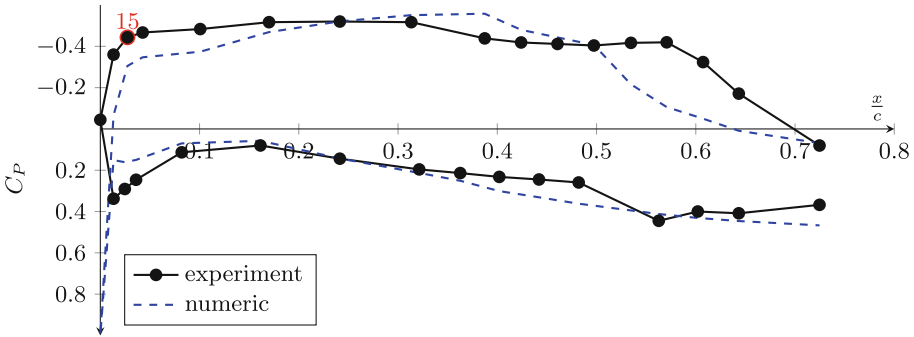

Fig. 7. Pressure distribution of the undeformed blade at $Re = 2.5 \cdot 10^5$, subsequent results shown for tap No. 15

Characterization of the static pressure distribution of the piezo adaptive blade was performed using 32 amplified differential low pressure sensors from First Sensor's HCLA series, specifically model designation HCLA0025DB. Each of the sensors has a measurement range of ± 25 mbar at a supply voltage of 5 V. The uncertainty of non-linearity and hysteresis is max. $\pm 0.25\%$ at full scale span. These sensors were placed outside the flow of the measuring section and connected to a long elastic tube and a short metallic tube inside the blade with orthogonal access to the point of interest perpendicular to the surface. The small metallic tubes have an inner diameter of 0.3 mm and a length of approx. 10 mm. The elastic tubes have an inner diameter of 1 mm and a length of approx. 3 m. The traveling pressure signals from the surface to the sensor within the elastic tube does not show much damping in a frequency range 120 Hz. The small inner diameter of the metallic tube but represents a challenge in this context because the whole tube cavity system has a high damping effect causing by wall friction. Consequently, a test bench was designed to calibrate the behavior of all of the tubes. With reference to [13] it is given with a linear approach by the transfer function

$$\mathbf{G}_t = \frac{1}{T_2 s^2 + T_1 s + 1}, \text{ with } T_2 = \frac{l\rho C}{A}, T_1 = \frac{k_1 C}{A}, k_1 = \frac{32\mu l}{d^2}, C = \frac{V}{\kappa P_0}, \quad (11)$$

with parameters given in table 4. By applying a binary signal to a magnetic valve with increasing frequency, the transfer function can be identified. As example of the measurements of all 32 tubes, an extract of the signal for the tube 15 is shown in Fig. 8. The measured input pressure signal is an oscillating signal with an overshoot. The output is damped because of the long traveling distance through the tube. At higher frequencies, the output is highly damped but the signal to noise ratio is high enough and a dynamic is still recognizable. Equation 11

Table 4. Data of tube system

Parameter	Symbol	Value	Unit
Average of the two tube diameters	d	0.6	mm
Average area	A	$2\pi(\frac{d}{2})^2$	mm^2
Volume of cavity taken from [13]	V	310	mm^3
Dynamic viscosity of air at 20 °C	μ	$18.2 \cdot 10^{-6}$	Pa s
Atmospheric pressure of air at 20 °C	P_0	1013	hPa
Heat capacity ratio	κ	1.4	–

is used for calibration with unknown tube length l. A simple gradient decent algorithm is used to fit the model to the data. As an example, Fig. 9 shows the fit for one tube. The values of the linear model deviate slightly from the measured data. After the calibration, the drop of amplitudes at high frequencies are out of the interesting range and thus they can be neglected. This backs the importance of frequency calibration. To suppress the amplifying effect of noise, the measured signal was first filtered with a butterworth low-pass filter of order 3. This is even more important because of the calibration mentioned above. Without filtering, the amplitudes of noise in particular would increase at high frequencies. To analyze the effect of throttling, the angle of incidence i_{CVC} was not be measured directly. The value of peak-to-peak pressure fluctuation $\hat{P}$ of all pressure taps were taken as comparable value for the throttling effect and the effect of the actuated blade.
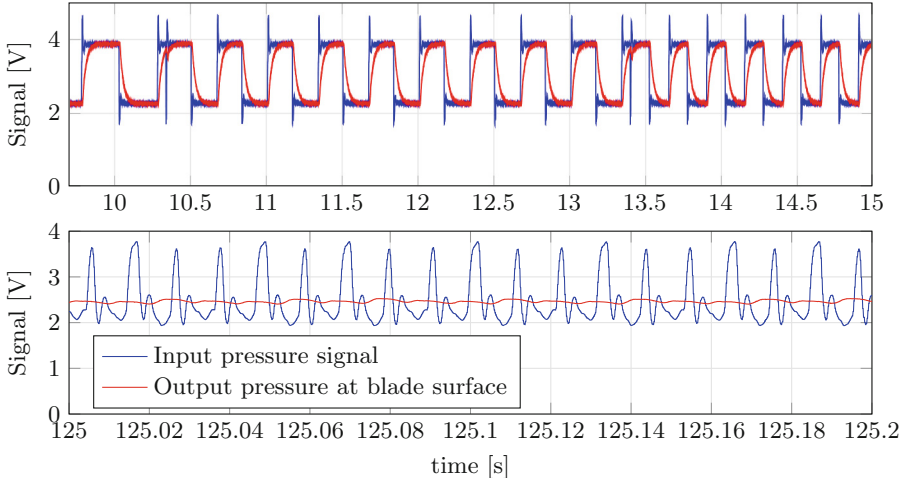

Fig. 8. Example sections of uncalibrated signals from pressure sensor of tap 15 to identify a transfer function from input to output for the tube frequency calibration; top from 2 4 Hz; 100 Hz
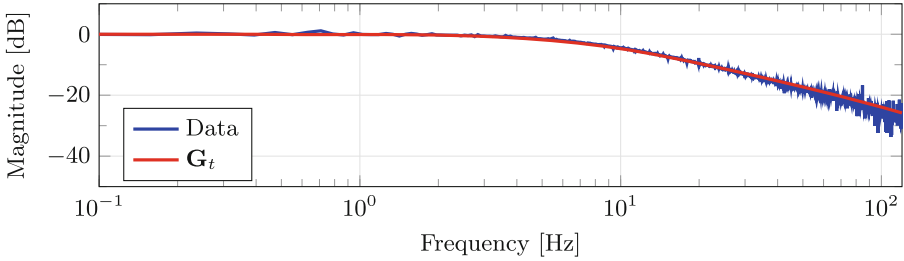
Fig. 9. Frequency response of the signal and fitted model for tube 15

5   Results

The peak-to-peak pressure fluctuation $\hat{P}$ at different throttling frequencies at one pressure tap (see Fig. 7) can be seen in Fig. 10. The behavior is comparable to wave propagation in a tube with fixed length and different boundary conditions as described in Eq. 11. The peak-to-peak pressure fluctuation drop at higher frequencies with proportion to the inverse of the frequency with all other parameters unchanged. This is the same behavior as the 20dB per decade pressure drop pictured in Fig. 9 starting at cutoff frequency because of the distance between throttling and measurement. It means that pressure fluctuations with high frequencies ($Sr > 0.144$) will not be recognizable at compressor stator stages with a distance to combustor of 5/3c.
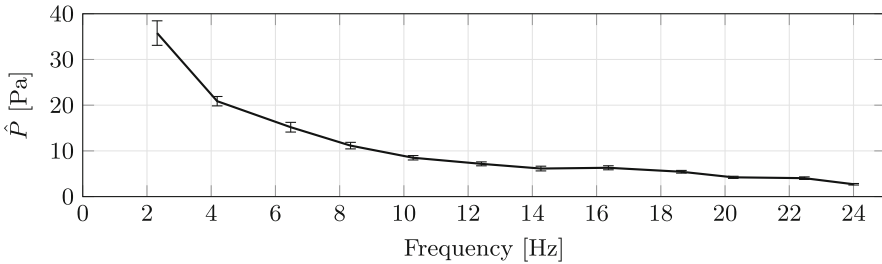

Fig. 10. Measurement results of the calibrated pressure fluctuation amplitudes and standard deviation for different throttling frequencies at tap 15 for a set of 50 measurements without actuation

Figure 11 shows an example of the averaged frequency spectrum of calibrated pressure measurements of tube 15 at an throttling frequency of $f_c = 24$ Hz ($Sr = 0.144$) from which the data for Fig. 10 was obtained. Although the fluctuations are in the hysteresis an non-linearity range, the fluctuation can be clearly measured. The second throttling frequency comes from averaging, since the throttling fluctuates, but this does not exceed two percent. The high amplitudes at twice and three times the throttling frequency are an indicator for an

additional disturbance of the rotating plates when they block the flow downstream again because of their rotating design. They are for this case higher than the throttling itself. However, there is no effect for four times the throttling frequency. It could also be an effect of the reflection of a pressure wave at the cascade and amplification after reflection.
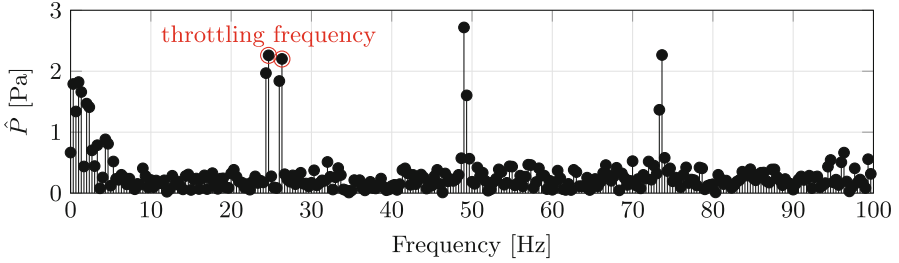

Fig. 11. Mean Fourier plot of pressure fluctuations measurements for throttling with $f = 24$ Hz and no actuation measured at tap 15 for a set of 50 measurements

In Fig. 12 depict the frequency responses of the strain gauge and the pressure sensor of tap 15. Resonance occurs at about $f_a = 61$ Hz. Furthermore, it can be seen that we can generate pressure amplitudes of up to $25 \, \text{Pa/dB}$ or about $18 \, \text{Pa}$ at resonance frequency with the piezo adaptive blade at this location. In addition the calculated frequency response of incidence angle i_{stat} after calibration at the structural test rig is shown. The result is similar to the calculated one also depict here. The frequency and magnitude of the first natural mode is driven by the choice of the material. Consequently lower natural frequencies and higher actuation magnitudes can be achieved with other materials. The highest impact on the flow can be achieved near by the first natural frequency due to a high deflection angle there. The second natural frequency is about twice as high and thus has no significant influence. It can be seen that the peak-to-peak pressure fluctuations reach a plateau between $f_a = 70$ Hz and the second natural frequency at around $f_a = 120$ Hz with values above the expected level. This effect results from the dynamic incidences described above and also seen in the calculated incidence angles in Fig. 2. It further shows, that pressure fluctuation of this high frequency could be extinguished.

Figures 13a to 13c shows the non actuated blade pressure distribution for min. and max. incidence at different throttling frequencies without any excitation of the blade to show the influence of throttling. Comparing the pressure distribution measurements at different angles of attack shown in [5,9], the angle of incidence at low frequency behaves like a change in the angle of attack. The differences between min and max almost disappear for high Strouhal numbers in throttling because of the reduced maximum effective incidence changes showed in Fig. 10. This means less instabilities at higher CVC-frequencies because of reduced i_{CVC}. The effect of only actuating the blade in resonance ($f_a = 61$ Hz,

$Sr = 0.366$) without any throttling but same flow conditions is shown in Fig. 13d. The min. and max. effect to the pressure distribution is comparable to throttling without actuation at $f_c = 10$ Hz ($Sr = 0.06$).
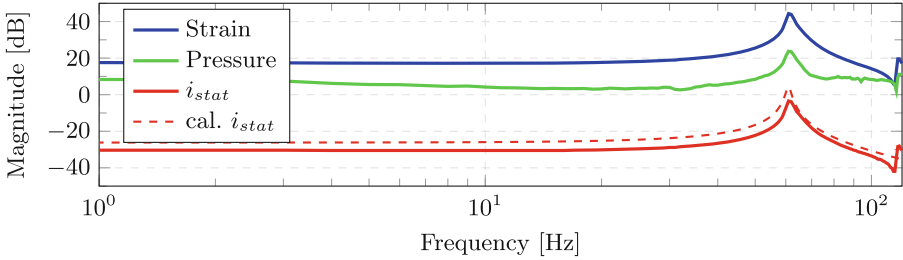

Fig. 12. Measured frequency response of static pressure at tap 15, strain gain and static incidence for the actuated blade

(a) Throttling with $f_c = 2$ Hz ($Sr = 0.012$)

(b) Throttling with $f_c = 10$ Hz ($Sr = 0.06$)

(c) Throttling with $f_c = 20$ Hz ($Sr = 0.12$)

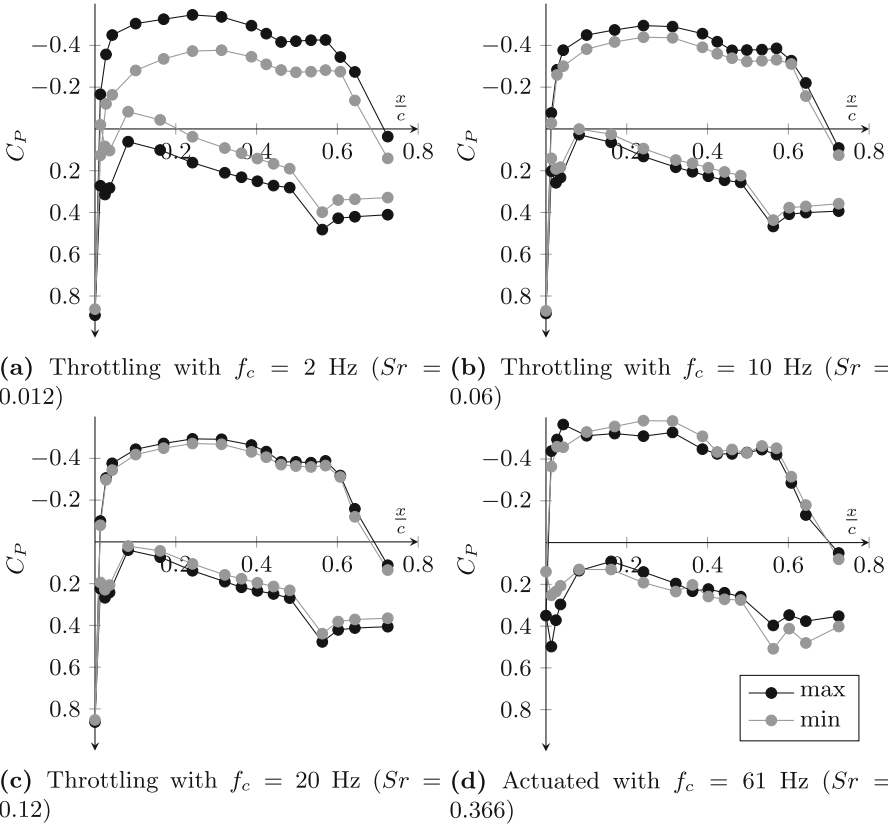**(d)** Actuated with $f_c = 61$ Hz ($Sr = 0.366$)

Fig. 13. Different pressure distribution of static blade with throttling and actuated blade without any throttling at $Re = 2.5 \cdot 10^5$ and different STROUHAL numbers

6   Conclusion

In this contribution, a piezo-adaptive blade in a periodically throttled stator cascade at high STROUHAL-numbers was demonstrated. MFC actuators on the inside of a hollow blade structure were used to bend the blade's front part covering in a high frequency range. A throttling device was used. By subsequent passage blocking, it generated pressure fluctuations mapping expected disturbances arising from a CVC process. These are causing incidence variations and thus an increased risk of choking or stalling. The effects of throttling and excitation were been demonstrated separately. The calculations in Sect. 2 and numerical results with other boundary conditions in [4] prove that both together leads to a resulting incidence i_{res} of nearly zero. Furthermore, this work shows that the effect of an excited aluminum piezo adaptive blade at the natural frequency is much higher than the effect of throttling at higher frequencies, seen in Fig. 13. A blade system with resonance near the CVC frequency could minimize the effect of throttling but the system properties have to be tailored very precisely and a control system could be necessary.

Looking at the pressure signal of the throttled case it is nearly harmonic. This means that a control system has only to excite the blade harmoniously with right voltage and phase shift. So it should be possible to design an easier open loop control system as an alternative to the previous work [8].

The experimentally obtained result shows that it is possible to minimize the effects of pressure gain combustion or other flow disturbances by adaptive blade morphing. An engine that uses this type of combustion to operate is most likely more effective. In summary, the actuation of the front part of a vane can reduce fluctuations in the pressure distribution without any compressed air. Further improvements in reducing fluctuations as well as raising static pressure behind the stage could be achieved with various blade designs and control systems.

References

1. Staats, M., Nitsche, W.: Active control of the corner separation on a highly loaded compressor cascade with periodic nonsteady boundary conditions by means of fluidic actuators. J. Turbomachinery **138**(3), 12, 031004 (2015)
2. Steinberg, S., King, R., Staats, M., Nitsche, W.: Iterative learning active flow control applied to a compressor stator cascade with periodic disturbances. J. Turbomachinery **137**(11), 111003 (2015)
3. Hammer, S., et al.: Active flow control by adaptive blade systems in periodic unsteady flow conditions. In: Active Flow and Combustion Control. Springer (2014)
4. Phan, T.D., Springer, P., Liebich, R.: Numerical investigation of an elastomer-piezo-adaptive blade for active flow control of a nonsteady flow field using fluid-structure interaction simulations. J. Turbomach. **139**(9), 04, 091004 (2017)

5. Phan, T.D.: Experimentelle und numerische Untersuchung des strukturdynamischen und strömungsmechanischen Verhaltens einer piezoadaptiven Verdichterschaufel zur Strömungsbeeinflussung. Doctoral thesis, Technische Universität Berlin (2019)

6. Krone, J.H., et al.: Experimental investigation and design of a shape-variable compressor cascade. CEAS Aeronaut. J. **8**(1), 105–127 (2017)

7. Ko, D., Guha, T.K., Amitay, M.: Control of reverse flow over a cantilevered blade using passive camber morphing. AIAA J. 1–22 (2021)

8. Werder, T., Liebich, R., Neuhäuser, K., Behnsen, C., King, R.: Active flow control utilizing an adaptive blade geometry and an extremum seeking algorithm at periodically transient boundary conditions. J. Turbomach. ***143***(2), 021008 (2021)

9. Steinert, W., Starken, H.: Off-design transition and separation behavior of a CDA cascade. J. Turbomach. **118**(2), 04, 204–210 (1996)

10. Bräunling, W.: Flugzeugtriebwerke. Springer, Heidelberg (2004). https://doi.org/10.1007/978-3-540-76370-3

11. Asahara, M., Kasahara, J., Matsuoka, K., Kawasaki, A., Matsuo, A., Funaki, I.: Pressure and visualization measurements on pulsed combustion thrustor. In: AIAA SciTech 2020 Forum, American Institute of Aeronautics and Astronautics (2020)

12. Anand, V., Gutmark, E.: Types of low frequency instabilities in rotating detonation combustors. In: King, R. (ed.) Active Flow and Combustion Control 2018, pp. 197–213. Springer, Cham (2019). https://doi.org/10.1007/978-3-319-98177-2_13

13. Kiesner, M.: Geregelte Strömungskontrolle einer Statorkaskade mit Seitenwand- und Hinterkantenaktuation. Doctoral thesis, Technische Universität Berlin, Berlin (2018)